PREDICTION OF ABRASIVE WEAR AND SURFACE HARDNESS OF PRINTED PARTS BY SLA TECHNOLOGY

PREDICCIÓN DE DESGASTE ABRASIVO Y DUREZA SUPERFICIAL DE PARTES IMPRESAS POR TECNOLOGÍA SLA

P. Muñoz-Valverde[1] , O. Villena-López[2] ,
L. Mayorga-Ases[2,*] , C. Pérez-Salinas[3] , D. Moya[3]

Abstract

In the present study, a prediction of hardness deterioration and abrasive wear was performed through a neural network using artificial intelligence on a material printed in SLA. This article aims to predict the mechanical properties, wear resistance and surface hardness of parts manufactured by SLA stereolithography printing. A full factorial DOE was used to associate the peculiar parameters (print orientation, cure time, layer height) to perform experiments. The mechanical properties were evaluated according to ASTM regulations, with the objective of obtaining feeding data and validation of the predictions of the Taber Wear Index and hardness using an artificial neural network. The experimental results are in good agreement with the measured data with satisfactory prediction errors with a mean square error (MSE) of 0.01 corresponding to abrasive wear using the clear resin and a mean absolute error (MSE) of 0.09 with an R2 of 0.756, the prediction with the neural network with a mean square error (MSE) of 2.47 corresponding to abrasive wear using the tough resin and a mean absolute error (MSE) of 14.3 with an R2 of 0.97. It was shown that the accuracy of the prediction is reasonable, and the network has the potential to be improved if the experimental database for training the network could be expanded. Therefore, wear and hardness mechanical properties can be predicted appropriately with an ANN.

Keywords: 3D printing, SLA Stereolithography, Taber wear index, surface hardness, artificial neural network, light-curing resins

Resumen

En el presente estudio se realizó una predicción del deterioro de la dureza y el desgaste abrasivo a través de una red neuronal utilizando inteligencia artificial sobre un material impreso en SLA. Esta investigación tiene como objetivo predecir las propiedades mecánicas de resistencia al desgaste y dureza superficial de piezas fabricadas mediante impresión por estereolitografía (SLA). Para realizar los experimentos se utilizó un diseño factorial de dos niveles o DOE factorial completo y así asociar los parámetros peculiares (orientación de impresión, tiempo de curado, altura de la capa). Las propiedades mecánicas fueron evaluadas según normativas ASTM, con el objetivo de obtener datos de alimentación y validación de las predicciones del índice de desgaste Taber y la dureza empleando una red neuronal artificial. Los resultados experimentales concuerdan con los datos medidos con errores de predicción satisfactorios con un error cuadrático medio (MSE) de 0,01 correspondiente al desgaste abrasivo utilizando la resina transparente y un error absoluto medio (MSE) de 0,09 con un R2 de 0,76. La predicción con la red neuronal tiene un error cuadrático medio (MSE) de 2.47 perteneciente al desgaste abrasivo utilizando la resina resistente y un error absoluto medio (MSE) de 14,3 con un R2 de 0,97. Se demostró que la precisión de la predicción es razonable, y que la red tiene potencial para mejorar si se pudiera ampliar la base de datos experimental para entrenar la red. Por lo tanto, las propiedades mecánicas de desgaste y dureza se pueden predecir, adecuadamente, con una RNA.

Palabras clave: impresión 3D, estereolitografía SLA, índice de desgaste Taber, dureza superficial, red neuronal artificial, resinas fotocurables

[1]Departamento de Ciencias Exactas, Universidad de las Fuerzas Armadas ESPE, Ecuador.
[2,*]Laboratorio de Materiales y Manufactura, Universidad Técnica de Ambato, Ecuador.
    Corresponding author ✉: la.mayorga@uta.edu.ec.
[3]Grupo de Investigación e Innovación en Ingeniería Mecánica GI3M-FICM, Universidad Técnica de Ambato, Ecuador.

1. Introduction

In recent years, additive manufacturing techniques have experienced accelerated progress in the development of prototyping and manufacturing in different fields [1–3]. Polymer printing has played a key role in this progress because its technology is widely available to developers. The new generation of printers has greatly boosted innovation, reducing the time and cost of product development. In addition, the use of additive manufacturing techniques in industry has become a field of great interest due to their high performance and ease of fabrication of complex three-dimensional geometrie.

The relatively low cost of commercially available 3D printers of different types allows the use of a wide range of materials with varying quality, precision, and resolution. Among the most common technologies, SLA (stereolithography) stands out, offering several advantages in precision applications, such as easy-to-use interfaces, resolution, and relatively fast printing speed [4–6].

The properties of SLA printed parts are intimately derived from the SLA process and post-process. In recent years, the mechanical properties obtained from SLA printed parts have been studied in the different light-curing resins available in the market. Even the improvement of the resins has been studied by evaluating the light curing process [7–9]. Properties such as tensile strength, tensile modulus, compressive strength were usually studied [10–12]. However, information on hardness and wear properties is scarce.

The surface hardness of polymeric materials is an important factor in their resistance to abrasive and adhesive wear. A polymeric material with a higher surface hardness will have a higher wear resistance, as it will be less prone to deformation, adhesion and material transfer during contact with abrasive or adhesive surfaces [13]. However, it is also important to consider other factors, such as the chemical structure of the polymer and its resistance to sliding and deformation, for a complete understanding of its tribological behavior [14]. SLA printed parts are increasingly used for engineering applications, where the wear phenomenon is an important aspect to consider. As hardness is a property that is related to the wear process, its inclusion in the analysis is also necessary. Studying the correlation between wear, hardness and SLA printing process parameters is important to design suitable compounds to meet various special requirements.

The prediction of mechanical properties is fundamental in the design of parts and components to ensure their proper functioning. The use of artificial neural networks (ANNs) to predict mechanical properties of materials has proven to be a very useful and powerful tool in engineering in different fields of manufacturing and specifically in wear-related issues [10], [15, 16].

ANNs can learn complex and nonlinear patterns from large data sets and therefore can accurately predict the mechanical properties of materials from limited information. This is especially useful when experimental data on the mechanical properties of a particular material is not available or when it is desired to reduce the time and costs associated with traditional mechanical testing. In summary, using ANN to predict mechanical properties is a valuable tool that can help engineers design more efficient and safer parts and components.

Neural network (NN) approaches are widely used methodologies reported in the literature among various machine learning techniques [17]. The ability of artificial NN to capture complex relationships between input and output data is valuable in manufacturing processes where it is difficult and expensive to obtain large experimental data for process modeling. In addition, NN models show an improvement in experimental error from 40% to 70% [18].

This paper studies the prediction of abrasion wear and hardness obtained from experimental tests on parts printed with thermosetting resins (tough and transparent resins) using SLA. The structure of this paper is as follows. First, the compilation on the technological properties of printed resins and the basics of printing is presented. Secondly, the analysis of hardness resistance and wear resistance of 3D printing by SLA stereolithography is provided by experiments. Finally, the abrasive wear during the 3D printing process is estimated using an artificial neural network based on the experimental data.

2. Materials and Methods

The presentation of this section is (1) the materials and their characteristics, (2) the experimental design, (3) the process of obtaining the printed material, (4) wear and hardness analysis of the tested items and (5) ANN prediction, as shown in the flowchart in Figure 1.

2.1. Materials

Two types of resins were used for property evaluation, Clear and Tough from $Formlabs^{TM}$. brand. Clear FLGPCL04 resin is used to print materials with high resolution and a smooth and soft finish [19]. Whereas Tough FLTOTL05 resin is used for solid prototyping because it balances strength and functionality. Both the manufacturer and printing service companies recommend its use in elements that are subjected to short periods of stress or fatigue [20], e.g., assemblies, press-type configurations and robust prototypes require the use of the aforementioned resin.

Table 1 summarizes the mechanical behavior of the material before and after curing, considering a treatment time of 60 min 60 °C, with a UV radiation of

1.25 mW/cm^2 and a wavelength of 405 nm for each type of resin. Nine properties are provided for Clear and Tough resin, the table is divided into three cate-gories, cured, uncured and the testing method used to determine each property.
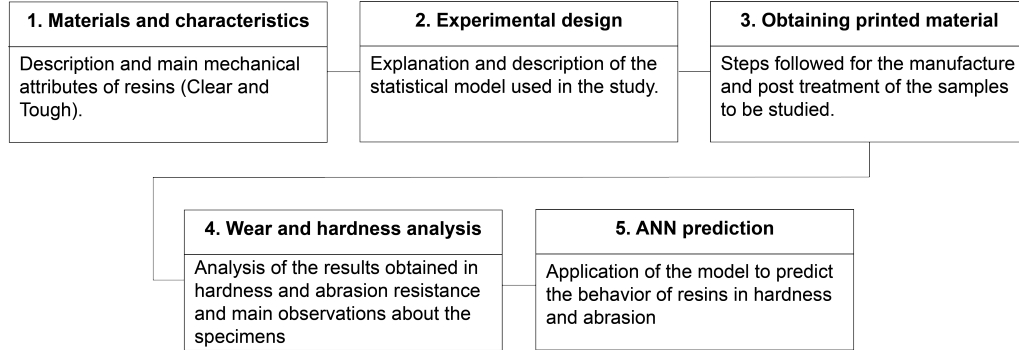

1. Materials and characteristics	2. Experimental design	3. Obtaining printed material
Description and main mechanical attributes of resins (Clear and Tough).	Explanation and description of the statistical model used in the study.	Steps followed for the manufacture and post treatment of the samples to be studied.

4. Wear and hardness analysis	5. ANN prediction
Analysis of the results obtained in hardness and abrasion resistance and main observations about the specimens	Application of the model to predict the behavior of resins in hardness and abrasion

Figure 1. Flow chart of the applied methodology.

Table 1. Mechanical properties of clear and tough resin [20, 21].

PARAMETERS	CLEAR RESIN			TOUGH RESIN		
	Uncured	Post - Cured	Method	Uncured	Post - Cured	Method
Ultimate Tensile Strength	38 MPa	65 MPa	ASTM D 638 - 10	34.1 MPa	55.7 MPa	ASTM D 638 - 14
Tensile Modulus	1.6 GPa	2.8 GPa	ASTM D 638 - 10	1.7 GPa	2.7 GPa	ASTM D 638 - 14
Flexural Stength at 5% Strain				42%	24%	ASTM D 638 - 14
Elongation at Failure	12%	6.2 %	ASTM D 638 - 10	20.8 MPa	60.6 MPa	ASTM C 790 - 15
Flexural Modulus	1.25 GPa	2.2 GPa	ASTM D 790 - 10	0.6 GPa	1.6 GPa	ASTM C 790 - 15
Notched IZOD	16 J/m	25 J/m	ASTM D 256 - 10	32.6 J/m	38 J/m	ASTM D 256 - 10
Heat Deflection Temperature (64 psi)	42.7 °C	58.4 °C	ASTM D 648 - 07	32.8 °C	45.9 °C	ASTM D 648 - 16
Heat Deflection Temperature (66 psi)	49.7 °C	73.1 °C	ASTM D 648 - 07	40.4 °C	48.5 °C	ASTM D 648 - 16
Thermal Expansion (23 - 50 °C)				1597 μm/m/°C	119.4 μm/m/°C	ASTM E 831 - 13

The considered mechanical properties are ultimate tensile strength, tensile modulus, flexural strength at 5% strain, elongation at failure, flexural modulus, notched IZOD, thermal deflection temperature at 64 Psi and 66 Psi and thermal expansion. The evaluation of the technological properties corresponds to the fluid absorption capabilities of the 3D printed parts, such as water, acetone or diesel. Fluid absorption is an important property of materials for medical devices due to their possible use as containers, flow conductors, etc.

Table 2 shows other properties such as the percentage weight gain from a 1x1x1 cm cube, the data correspond to the two resins in 24 hours of immersion in different solvents.

The tensile behaviour of the two resins considering different curing times is shown in Figure 2. Due to their good tensile behaviour, both resins can be used for printing mechanical parts. For example, the Tough resin is used to print gears for RC prototypes, [22]. On the other hand, Clear resin, thanks to its high surface quality, offers the possibility of being used on visually exposed elements. In addition, replacement on any device is easier, as the affected elements can be replaced in a short time with a new one thanks to this printing technology.

Table 2. Percentage weight gain of the two resins in 24 hours of immersion in different fluids of a 1x1x1 cm cube, [20, 21].

| SOLVENT	CLEAR	TOUGH
	Gain (%)	
Strong Acid (HCl)	Distores	Distored
Xylene	< 1	< 1
Water	< 1	1.6
Sodium hydroxide (0.0025% - PH = 10)	< 1	1.5
Salt Water (3.5%)	< 1	1.5
Mineral Oil (Heavy)	< 1	< 1
Mineral Oil (Ligth)	< 1	< 1
Isooctane	< 1	< 1
Hydrogen Peroxide (3%)	< 1	2.1
Acetic Acid (5%)	< 1	2.8
Acetone	Sample cracked	Sample cracked
Isopropyl Acetate	< 1	2.1
Bleanch (5% aprox)	< 1	1.7
Butyl Acetane	< 1	1.6
Diesel	< 1	< 1
Diethyl glicol monomethyl ether	1.7	6.6
Hydrolic Oil	< 1	< 1
Skydrol 5	1	1.2
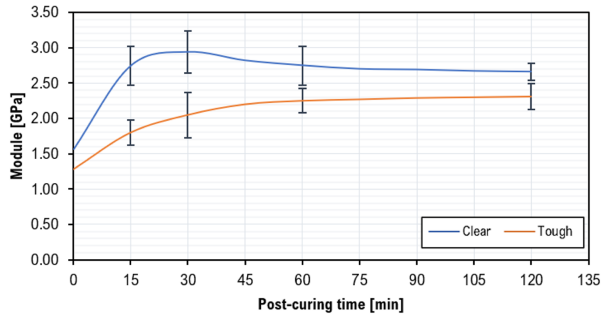
Figure 2. Young modulus vs post cured time for the Clear and Tough Resin

2.2. Experimental design

The orthogonal matrix, in the context of a statistical study, is a tool used to study and analyse all variables independently and simultaneously. It allows the analysis of one variable to be unaffected by the other variables in the study, making it easier to study each variable separately and understand its individual impact. This is due to the independence of data in the study.

By analysing variables independently, the possibility of introducing bias or confounding between them is reduced. This helps to obtain more reliable and accurate results because each variable is examined in isolation and potential sources of error can be better identified and controlled.

Consequently, an orthogonal matrix experimental design was applied in which two quantitative variables (curing time and impression orientation) and a qualitative variable corresponding to resin type were used with three levels as presented in Table 3.

Table 3. Experimental design

| FACTORS | UNIT | LEVEL 1 | | LEVEL 2 | | LEVEL 3 | |
		T	C	T	C	T	C
Curing time	[min]	0	0	15	60	30	120
Print orientation	[°]	0		45		-	
Resin type	-	Tough (T)		Clear (C)		-	

In this analysis, a distribution of the data from a full factorial model was used. The number of experimental runs was set to 5. 100 combinations of experimental data were obtained. The data were cleaned for the existence of null values, especially for the Tough resin with 15 and 30 minutes curing times and the Clear resin with 60 and 120 minutes curing times.

2.3. Process of obtaining printed material

Figure 3 shows a SIPOC diagram of the process carried out for the printing of the specimens with the material proposed for the analysis. The graph details the steps (1) to (5) that correspond to the inputs and prototyping, while step (6) details the tests that were carried out for the analysis and data collection that fed the neural network.

Initially, the resins are in a liquid state, stored and supplied from cartridges (1). The specimens were then modelled using design software (2). For printing, the parameters specified by the manufacturer were followed [23] and the variables described in the experimental design were set (3).

The fabrication of each specimen from the SLA process was carried out by means of the printing phase in the Form 2 SLA machine considering the experimental design guidelines, the washing phase was carried out in the Form Wash machine with isopropyl alcohol solvent for a period of 10 to 20 minutes (4) and finally, the curing was carried out in the Form Cure machine.

For the curing stage of the specimens, a time span of 0 to 30 minutes was taken into consideration for the Clear resin and 0 to 120 minutes for the Tough resin as specified in Table 3 (5). An estimate of the time that can be spent per layer can be obtained from Equation (1). The forming time (Tc) depends on the area of the layer to be formed (Ac), the speed (v) and the diameter (D) of the beam, plus the repositioning time for layer materialisation (Tr). The sum of the formation time of each layer gives the total processing time, [24].

$$Tc = \frac{Ac}{vD} + Tr \qquad (1)$$

In general terms, the SLA 3D printing process can be mathematically defined by relationships such as the depth of cure, the width of the cure line and the laser exposure at any point.

The depth of cure ratio (Equation (2)) is related by the laser penetration depth (Dp), the exposure energy at the resin surface (Eo) and the minimum energy to gel the resin (Ec) [24]. The width of the cured line (Lw) is expressed by Equation (3). In this relation, D is equivalent to the diameter of the laser in use in the printing machine.

$$Cd = Dp\, Ln\left(\frac{Eo}{Ec}\right) \qquad (2)$$

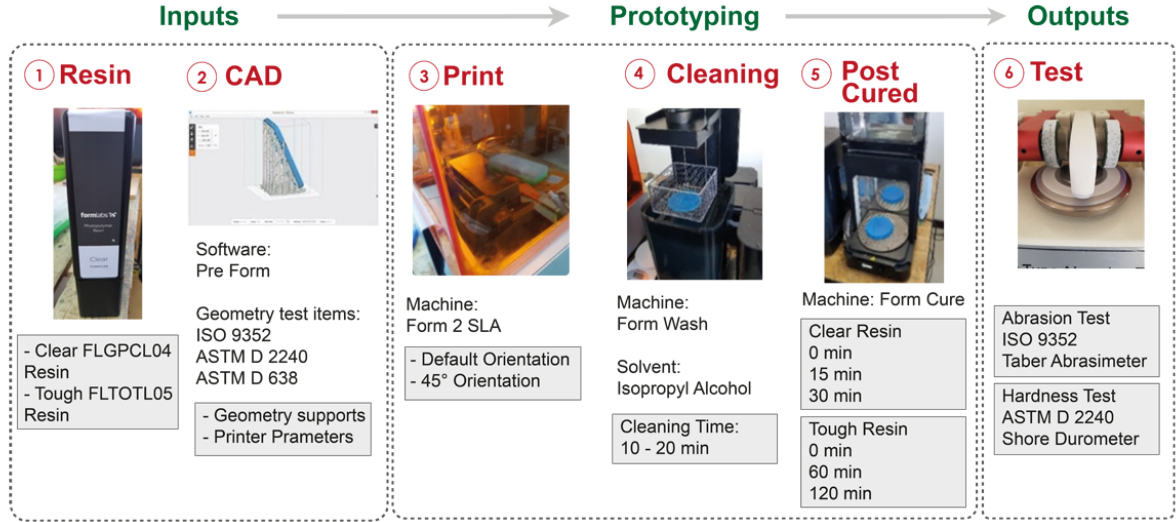$$Lw = D\sqrt{\frac{Cd}{2Dp}} \qquad (3)$$

Figure 3. Stages in obtaining printed material for analysis

Considering that the laser has motions in all 3 axes (X - Y - Z), the laser exposure at any point (E (x, y, z)) is determined by Equation (4). The point (x, y) represents the distance from the centre to the beam, (z) the depth at which it is located, (Pl) is equal to the laser power, the Gaussian mean width (Wo) Vs the laser scanning speed and (Dp) the laser penetration depth, [25].

$$E(x, y, z) = \sqrt{\frac{2}{\pi}} \ \frac{Pl}{WoVs} \ e^{-\frac{2y^2}{Wo^2}} \ e^{-\frac{z}{Dp}} \quad (4)$$

Isotropy is a critical characteristic that relates to the parameters defined by Equations 1-4. Isotropy is one of the consequences of post-curing, which strengthens the bonds by forming covalent bonds. At the micro level, there is no marked difference between molecules arranged in the X - Y - Z planes. This makes its mechanical performance predictable and therefore better than other types of 3D printing. On the other hand, impermeability is another characteristic that outperforms the material after curing. This distinctive feature is one of the reasons why this type of printing is often used when dealing with fluids.

2.4. Wear and hardness analysis of tested items

Following the indications set out in the ISO 9352 standard. A load of 1000 grams and 1000 cycles were applied at a speed of 72 rpm. The type of grinding wheel used was intermediate grade H22. The reported result is the Taber Wear Index (TWI), Equation (5), where A is the weight of the sample before the test, B is the weight of the sample after the test and C is equal to the number of cycles used in the test.

$$TWI = \frac{[(A - B)1000]}{C} \quad (5)$$

Each test specimen was tested, and the results are expressed in terms of a Shore D hardness unit, which represents the resistance of the material to penetration by the test needle. On the Shore D scale, lower hardness values correspond to softer materials and higher values correspond to harder materials. The Shore D scale is particularly suitable for rigid materials, with a typical hardness range of 20 to 90 Shore D.

2.5. Artificial neural network (ANN) analysis methods

A neural network is a technique inspired by the biological nervous system, which aims to replicate the way humans learn to solve a wide variety of complex scientific problems. Neural networks consist of several layers of neurons connected with synaptic weights to simulate the human brain. A simplified network consists of an input layer with a number of neurons depending on the input variables (3 in this study), followed by one or more hidden layers that transform those variables for final use in the output layer [26, 27].

Overfitting is a problem related to neural network training. According to research [28–30], determine that too few neurons lead to underfitting, while too many neurons can contribute to overfitting.

Figure 4 shows the neural scheme used, where W is the synaptic weight from each neuron to another neuron in the next layer.
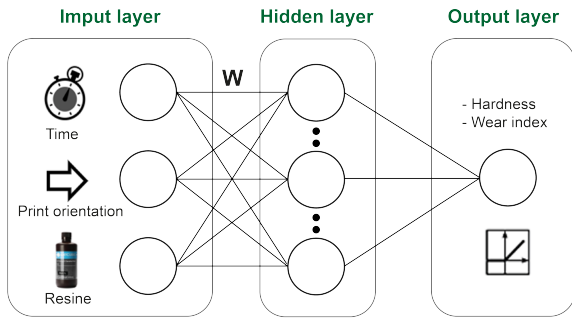
Figure 4. Neural network architecture with three layers implemented from the input to the output layer.

The multilayer feed forward network architecture used in this study consists of three neurons for the input layer, which are ordered according to the number of input variables. One neuron is in the output layer (abrasive wear) and two are hidden layers with ninety-six neurons each. The selected number of neurons in the hidden layer is determined by a trial and error procedure. To decrease the difficulty of training and to balance the importance of each parameter during the training process, the experimental database was normalised between the values 0 and 1.

The scaling of the input and output variables in the interval is determined by the ratio of the difference of the input and output variables. The scaling of the input and output variables in the interval is determined by the ratio of the difference of the input data to the mean and standard deviation (Equation (6)), where x is a data point, μ is the mean and σ is the standard deviation.

$$z = \frac{x - \mu}{\sigma} \qquad (6)$$

The output of each neuron of the hidden and output layers is given by the function ReLU. This function represents the activation fusion (Equation (7)). Adam's optimisation algorithm was used together with the backpropagation training algorithm [31] to train the multilayer neural network and calculate the gradient required for weight adjustment.

$$\sigma(x) = \begin{cases} x \ si \ x \geq 0; \\ x \ si \ x < 0; \end{cases} \qquad (7)$$

The training phase of the ANN determines the connection weights needed to give the desired response. The first step is to assign random weight values to all links between neurons. Next, the parameter values of the k-th experiment from the training data list are passed through the network. The estimated value is compared with the desired value using the functions: mean square error (MSE) and mean absolute error (MAE).

The different weights connecting the elements in the neural network are adjusted and approached to the target output value. Equation (8) represents the update of the synaptic weights, based on the calculated error in each neuron.

$$w'ji(n) = wji(n) + \Delta wji(n) \qquad (8)$$

Where $w'ji(n)$ represent the adjusted weights, $wji(n)$ are the previous weights and $\Delta wji(n)$ is the synaptic weight correction. After updating all weights according to the training error, an epoch (n) is completed. An epoch is when all training trials (60 for this study) are evaluated. If the MSE is not lower than a specific target, the process is repeated by updating the weights and increasing the number of epochs required until the target is reached.

3. Results and discussion

The results are reported in two stages, (1) experimental analysis of influential factors on the output variables (Taber wear index and hardness) and (2) wear prediction by neural network.

3.1. Experimental analysis of output variables

Figure 5 details the specimens subjected to the abrasion test where the topology of the specimens has undergone a noticeable change. The main evidence is shown in the quality of the track left by the grinding wheel. This is consistent with the results presented, which indicate that there is a 70% difference in mass loss between the white (Clear Resin) and blue (Tough Resin) specimens. The latter being the most resistant to abrasion.
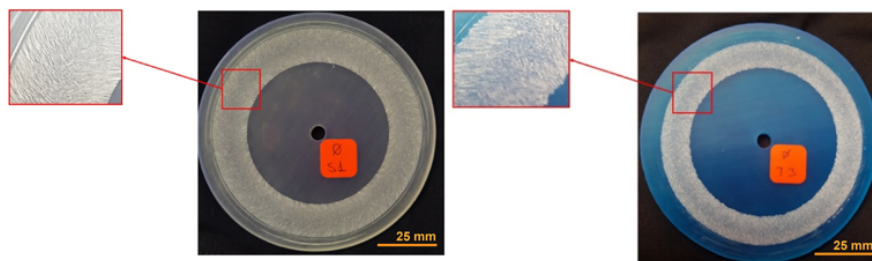

Figure 5. Tested specimens - wear resistance.

On the other hand, regarding the hardness test, it can be said that the hardness scale of the resins increases as the curing time increases. In other words, there is a directly proportional relationship. The Clear resin presents its maximum peak of Shore D hardness at 15 minutes of curing with an average of 88.4, being the highest among the two resins used in the study. The Tough resin presents its maximum peak at 60 minutes of cure with an average hardness scale of 78.6.

Table 4 shows the distribution of the data from a full factorial model.

Table 4. Training data. Full Factorial model with 5 experimental runs

N°	CURED [min]	ORIENTATION [°]	ABRASION	CLEAR RESIN	TOUGH RESIN	N°	CURED [min]	ORIENTATION [°]	ABRASION	CLEAR RESIN	TOUGH RESIN
1	30	0	0.73	1.00	0.00	31	60	45	0.06	0.00	1.00
2	30	45	0.43	1.00	0.00	32	60	45	0.08	0.00	1.00
3	120	45	0.11	0.00	1.00	33	0	45	0.06	1.00	0.00
4	15	0	0.69	1.00	0.00	34	60	45	0.12	0.00	1.00
5	120	0	0.57	0.00	1.00	35	0	45	0.64	1.00	0.00
6	60	0	0.36	0.00	1.00	36	15	0	0.45	1.00	0.00
7	0	45	0.64	1.00	0.00	37	30	0	0.52	1.00	0.00
8	0	0	11.80	1.00	0.00	38	0	0	11.80	1.00	0.00
9	30	0	0.52	1.00	0.00	39	30	45	0.31	1.00	0.00
10	0	0	0.74	0.00	1.00	40	0	45	0.31	0.00	1.00
11	0	0	0.88	0.00	1.00	41	0	0	0.64	0.00	1.00
12	120	45	0.06	0.00	1.00	42	30	45	0.36	1.00	0.00
13	0	0	0.90	0.00	1.00	43	120	0	0.48	0.00	1.00
14	15	45	0.33	1.00	0.00	44	15	45	0.41	1.00	0.00
15	60	0	0.43	0.00	1.00	45	15	45	0.45	1.00	0.00
16	30	45	0.50	1.00	0.00	46	0	45	0.27	0.00	1.00
17	0	0	11.80	1.00	0.00	47	15	0	0.43	1.00	0.00
18	120	45	0.10	0.00	1.00	48	30	0	0.70	1.00	0.00
19	0	45	0.64	1.00	0.00	49	15	0	0.96	1.00	0.00
20	0	45	0.29	0.00	1.00	50	0	0	11.80	1.00	0.00
21	60	45	0.14	0.00	1.00	51	120	0	0.41	0.00	1.00
22	120	45	0.08	0.00	1.00	52	120	45	0.09	0.00	1.00
23	15	45	0.49	1.00	0.00	53	0	0	0.72	0.00	1.00
24	120	0	0.48	0.00	1.00	54	60	45	0.15	0.00	1.00
25	30	0	0.47	1.00	0.00	55	0	45	0.18	0.00	1.00
26	15	45	0.49	1.00	0.00	56	0	45	0.21	0.00	1.00
27	60	0	0.37	0.00	1.00	57	60	0	0.50	0.00	1.00
28	0	45	0.64	1.00	0.00	58	30	45	0.45	1.00	0.00
29	15	0	0.43	1.00	0.00	59	0	0	11.80	1.00	0.00
30	60	0	0.49	0.00	1.00	60	120	0	0.33	0.00	1.00

Figure 6 shows the experimental results for the main effects of hardness and wear rate at 5% significance level. For hardness (Figure 6a), it is observed that both resin type and curing time are incident variables (p-value < 0.01 for the two factors in the ANOVA analysis). Impression orientation is not incident (p-value > 0.01). On the other hand, figure 6b shows that all factors (resin type, curing time and impression orientation) are incident on abrasion resistance (p-value < 0.01) for all factors. For both response variables, the resin with the highest performance is Clear resin.
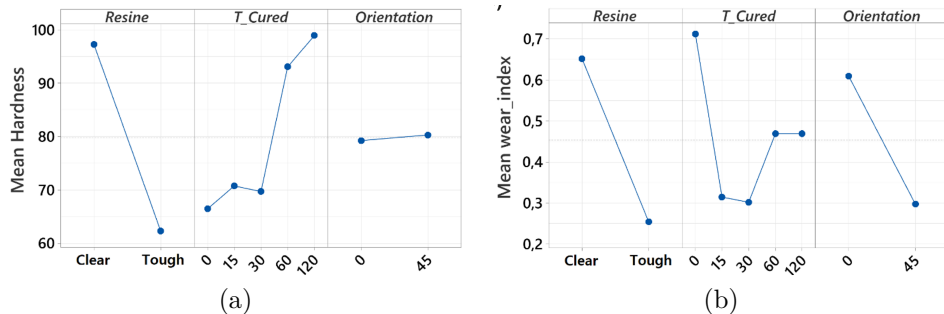

Figure 6. Main effects plot. a) Hardness, b) Abrasion resistance - Tabber test

Figure 7 shows the hardness behaviour of the two resins (Clear, Tough Resin) as a function of curing time; (figure 7a), corresponding to the Clear resin, shows a higher hardness. However, the highest values are in the range of 15 to 30 minutes. On the other hand, a similar behaviour is observed in the Tough resin (figure 7b), where it is evident that the longer the curing time, the higher the hardness. To achieve these results, a curing range of 60 minutes is necessary. It is also observed that the recommended curing time should not be exceeded because it does not improve the hardness of the material.

Figure 8 shows the abrasion results. The two resins have a distinct pattern of behaviour. As they are not cured, they do not show good stability (low strength). The abrasion resistance increases when the two resins are cured for the first time. Regardless of the time, it is observed that the change is noticeable between 0 min and 5 min (Resin Clear 8a). Thereafter, as shown by the tensile strength results, the values do not show noticeable changes. In other words, the longer the curing time, the higher the abrasion resistance.
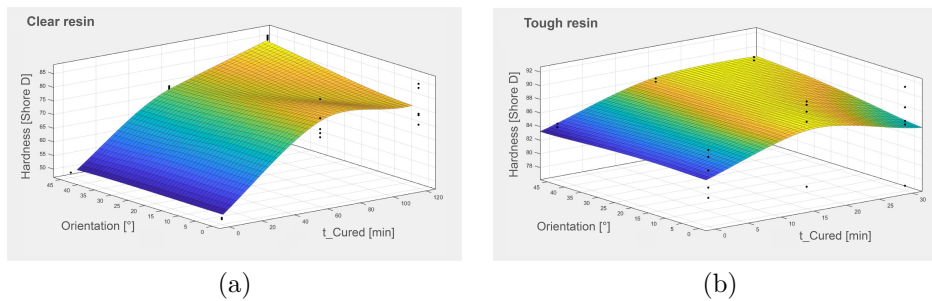

(a)　(b)

Figure 7. Experimental results. (a) Clear Resin: Hardness vs Orientation vs Post – Cured (b) Tough Resin. Hardness vs Post Cured time Vs Orientation.
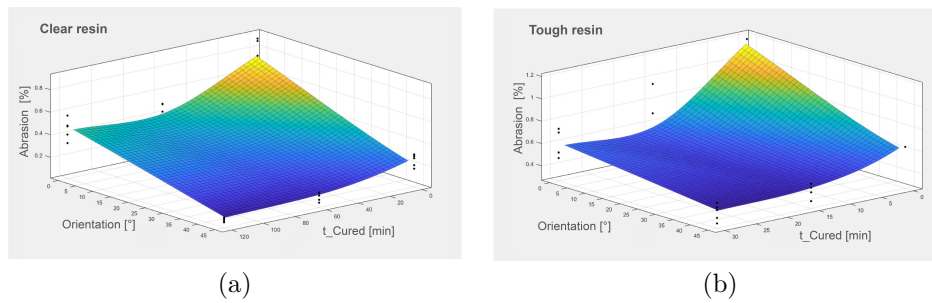

(a)　(b)

Figure 8. Experimental results. (a) Clear Resin: Wear resistance vs Orientation vs Post – Cured (b) Tough Resin. Wear resistance vs Post Cured time Vs Orientation.

3.2. Abrasive wear and hardness prediction by artificial neural network

A neural model was developed to estimate the Taber wear rate (TDI) and hardness based on different combinations of stereolithographic 3D printing. The database was obtained through laboratory tests. The experimental data used for the training stage was divided by cross-validation into 80% for training and 20% for validation. It was developed with a feed - forward and back propagation neural scheme on a total of 60 experimental data.

The best performing model was the 5-96-96-1 architecture. The activation function ReLu was used for both the hidden layers and the output layer. Figure 9 shows the relationship between the values obtained by neural training and the values obtained experimentally.

The evolution of the MAE and MSE with the epochs for the designed neural network is presented in Figure 10, where the convergence of the results is observed. The MAE at the end of the abrasive wear training procedure resulted to be 0.09 using Clear resin and an MSE value of 0.01. To measure the accuracy of the ANN, the correlation coefficient (R^2) between the results and the targets was calculated. In this case, $R^2 = 0.75$ represents a correlation between experimental and estimated values. The MAE is 2.47 using tough resin and an MSE value of 14.3. The correlation coefficient (R^2) between the results and the targets was calculated. In this case, $R^2 = 0.97$.

MAE evaluated the predictive performance of the model, MSE and R^2 values. Previous research [26], [32, 33] recommends that the model should have high

R2 and low MAE and MSE for the neural model to have high efficiency. Figure 11 shows the results of the ANN training process after reaching the minimum gradient. Table 5 presents the results of MAE and MSE after network training.
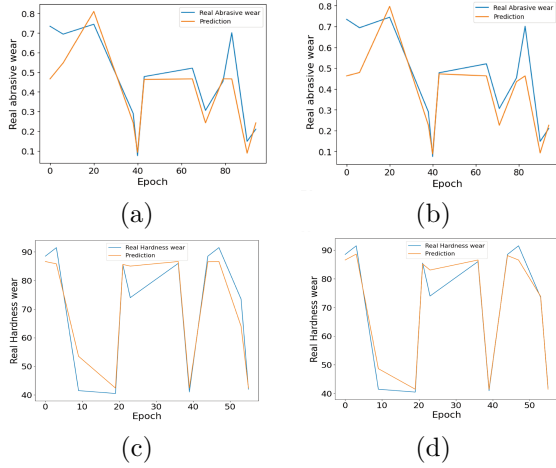

Figure 9. Overall comparison between predicted and experimental values of abrasive wear. a) Abrasive wear with Clear Resin b) Abrasive wear with Tough Resin c) Hardness with Clear Resin d) Hardness with Tough Resin
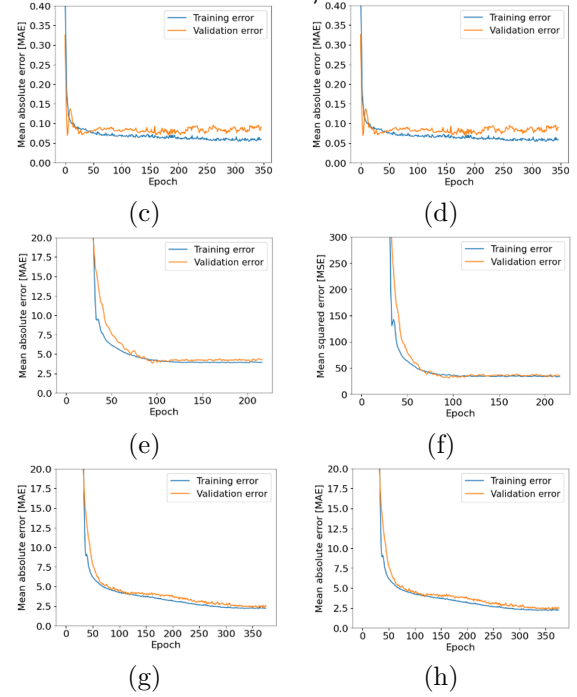

Figure 10. Evolution of the mean absolute error and evolution of the mean squared error with the number of epochs. a) MAE of abrasive wear with Clear Resin b) MSE of abrasive wear with Clear Resin c) MAE of abrasive wear with Tough Resin d) MSE of abrasive wear with Tough Resin e) MAE of hardness with Clear Resin f) MSE of hardness with Clear Resin g) MAE of hardness with Tough Resin h) MSE of hardness with Tough Resin
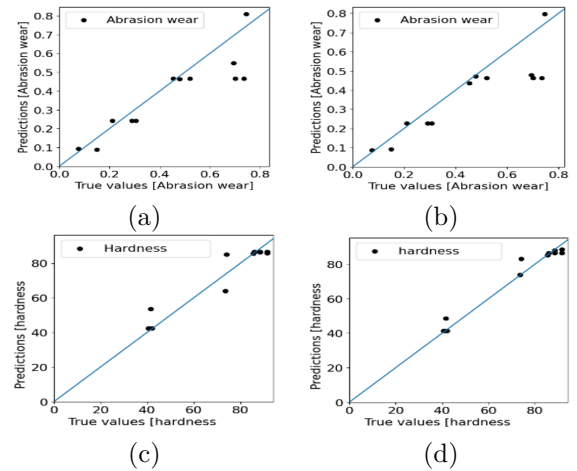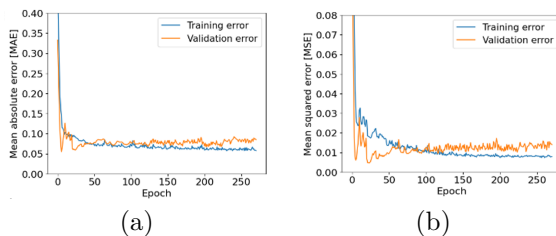
Table 5. MAE, MSE and R2 statistics of the neural model

DATA SET	MAE	MSE	R^2
Abrasive wear of Clear resin			
Training	0.06	0.01	
Validation	0.09	0.01	0.75
Tough resin abrasive wear			
Training	0.06	0.01	
Validation	0.09	0.02	0.69
Clear resin hardness			
Training	3.88	33.48	
Validation	4.28	35.46	0.92
Tough resin hardness			
Training	2.17	14.41	
Validation	2.47	14.33	0.97

Figure 11. Regression between the data presented by the neural network and the real values obtained experimentally for abrasive wear. a) Abrasive wear with Clear Resin b) Abrasive wear with Tough Resin c) Hardness with Clear Resin d) Hardness with Tough Resin

Table 6 presents the best hyperparameter settings for the neural model, considering the statistical results and computational cost.

Figure 12 illustrates the distribution of the residuals of the model. Most of the residuals are close to zero, which determines the satisfactory performance of the proposed neural network model. The residuals are not close to a normal curve. This behavior may be due to the small sample size considered for training.
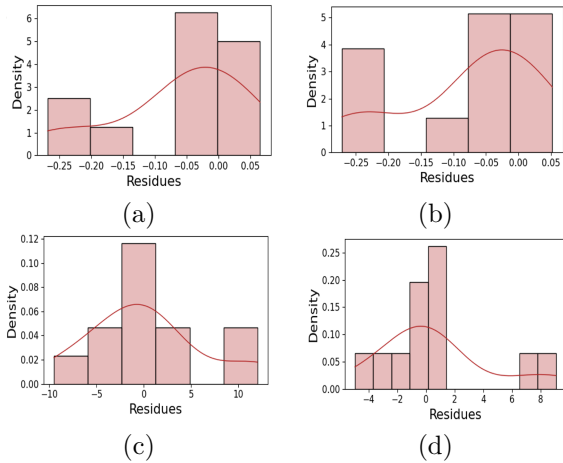

(a)

(b)

(c)

(d)

Figure 12. The distribution plot of residuals tends to a Gaussian curve, i.e. most of the residuals tend to approach the value of zero. a) Abrasive wear Clear Resin b) Abrasive wear with Tough Resin c) Hardness with Clear Resin d) Hardness with Tough Resin

Table 6. Hyperparameters of the neural network model

PARAMETER	VALUE
Network architecture	5 - 96 - 96 - 1
Input parameters	- Resin type - Curing time - Print orientation
Output parameters	Taber wear index (IWT) and hardness
Activation function	ReLu
Optimiser	Adán
Performance function	- Mean sqare error (MSE) - Mean absolute error (MAE) - Coefficient of determination (R2)
Learning rate	0.001
Number of iterations	500
Batch size	10

The prediction of the network was determined through the estimated values during the validation of the neural network model. However, it is observed that several values do not agree with the real data. This problem could be caused by the following three factors: type of material, lack of sampling accuracy and the architecture of the neural network.

Table 7 represents the percentage error presented by the network on each validation data. The results indicate the similarities between the experimental studies and the neural model, supporting the reliability of the model.

Table 7. Abrasion rate of the prediction error compared to actual values

DATA SET	% ERROR
Clear resin abrasive wear	19.34
Tough resin abrasive wear	19.60
Clear resin hardness	6.87
Tough resin hardness	3.92

4. Conclusions

The first objective is related to the analysis of the mechanical properties of the resins, it was determined that hardness and stress increase as a function of the post-curing time of each resin. The Tough and Clear resins have shown a definite pattern in their behavior, especially in hardness and abrasion. When uncured, their properties are lower than when cured at 60 min, which is in line with the manufacturer's recommendations. This jump is very noticeable especially in hardness and tensile strength. If the curing time is increased, their properties have a negligible increase. After the maximum curing time of 120 min, there will be no appreciable improvement in properties.

The neural network model successfully predicted the experimental results with a mean square error of 0.014 and a mean absolute error of 0.085 using clear resin. The MAE is 2.27 using tough resin and an MSE value of 14.33. The correlation coefficient (R^2) between the results and the targets was calculated. In this case, $R^2 = 0.97$. This shows that the predicted results agree with the measured values. It is also verified that the artificial neural network model is reliable and that the predicted results provide useful information for developing new abrasive wear resistant materials.

The visual surface diagrams constructed with the network results can be used to monitor the impact of wear evolution, reduce damage, and prevent component fracture. Finally, it is concluded that SLA 3D printing with Clear and Tough resins are good alternatives for use in the printing of emerging components due to their hardness and good abrasive wear behavior.

The abrasion experiment is limited to a medium grade. Due to the use of grinding wheels of the type mentioned above. As there is a specific degree of abrasion, the experimental conditions are limited to those proposed by the ISO 9352 abrasion standard. If it is necessary to know the behavior of the material under high and low abrasion, it is advisable to conduct experiments using grinding wheels that meet the requirements.

Acknowledgements

References

[1] T. D. Ngo, A. Kashani, G. Imbalzano, K. T. Nguyen, and D. Hui, "Additive manufacturing (3D printing): A review of materials, methods, applications and challenges," *Composites Part B: Engineering*, vol. 143, pp. 172–196, 2018. [Online]. Available: https://doi.org/10.1016/j.compositesb.2018.02.012

[2] A. I. Pérez Sanpablo, E. Romero Avila, and A. González Mendoza, "Three-dimensional printing in healthcare," *Revista Mexicana de Ingenieria Biomedica*, vol. 42, no. 2, pp. 32–48, 2021. [Online]. Available: https://doi.org/10.17488/RMIB.42.2.3

[3] T. Wohlers, *Rapid Prototyping & Tooling State of the Industry Annual Worldwide Progress Report Wohlers Report.* Wohlers Associates, 2001. [Online]. Available: https://bit.ly/46DJYlv

[4] E. J. Hurst, "3D printing in healthcare: Emerging applications," *Journal of Hospital Librarianship*, vol. 16, no. 3, pp. 255–267, 2016. [Online]. Available: https://doi.org/10.1080/15323269.2016.1188042

[5] S. Mishra, "Application of 3D printing in medicine," *Indian Heart Journal*, vol. 68, no. 1, pp. 108–109, 2016. [Online]. Available: https://doi.org/10.1016/j.ihj.2016.01.009

[6] J. W. Stansbury and M. J. Idacavage, "3D printing with polymers: Challenges among expanding options and opportunities," *Dental Materials*, vol. 32, no. 1, pp. 54–64, 2016. [Online]. Available: https://doi.org/10.1016/j.dental.2015.09.018

[7] A. C. Uzcategui, A. Muralidharan, V. L. Ferguson, S. J. Bryant, and R. R. McLeod, "Understanding and improving mechanical properties in 3D printed parts using a dual-cure acrylate-based resin for stereolithography," *Advanced Engineering Materials*, vol. 20, no. 12, p. 1800876, 2018. [Online]. Available: https://doi.org/10.1002/adem.201800876

[8] C. Mendes-Felipe, D. Patrocinio, J. M. Laza, L. Ruiz-Rubio, and J. L. Vilas-Vilela, "Evaluation of postcuring process on the thermal and mechanical properties of the Clear02 resin used in stereolithography," *Polymer Testing*, vol. 72, pp. 115–121, 2018. [Online]. Available: https://doi.org/10.1016/j.polymertesting.2018.10.018

[9] A. Bardelcik, S. Yang, F. Alderson, and A. Gadsden, "The effect of wash treatment on the mechanical properties and energy absorption potential of a 3D printed polymethyl methacrylate (pmma)," *Materials Today Communications*, vol. 26, p. 101728, 2021. [Online]. Available: https://doi.org/10.1016/j.mtcomm.2020.101728

[10] Z. Jiang, Z. Zhang, and K. Friedrich, "Prediction on wear properties of polymer composites with artificial neural networks," *Composites Science and Technology*, vol. 67, no. 2, pp. 168–176, 2007, modelling and Characterization of Composites. [Online]. Available: https://doi.org/10.1016/j.compscitech.2006.07.026

[11] A. D. Tura, H. G. Lemu, H. B. Mamo, and A. J. Santhosh, "Prediction of tensile strength in fused deposition modeling process using artificial neural network and fuzzy logic," *Progress in Additive Manufacturing*, vol. 8, no. 3, pp. 529–539, Jun 2023. [Online]. Available: https://doi.org/10.1007/s40964-022-00346-y

[12] M. Tayyab, S. Ahmad, M. J. Akhtar, P. M. Sathikh, and R. M. Singari, "Prediction of mechanical properties for acrylonitrile-butadiene-styrene parts manufactured by fused deposition modelling using artificial neural network and genetic algorithm," *International Journal of Computer Integrated Manufacturing*, vol. 36, no. 9, pp. 1295–1312, 2023. [Online]. Available: https://doi.org/10.1080/0951192X.2022.2104462

[13] U. S. Tewari, S. K. Sharma, and P. Vasudevan, "Polymer tribology," *Journal of Macromolecular Science, Part C*, vol. 29, no. 1, pp. 1–38, 1989. [Online]. Available: https://doi.org/10.1080/07366578908055162

[14] B. Gupta, "3 - friction and wear mechanism of polymers, their composites and nanocomposites," in *Tribology of Polymers, Polymer Composites, and Polymer Nanocomposites*, ser. Elsevier Series on Tribology and Surface Engineering, S. C. George, J. T. Haponiuk, S. Thomas, R. Reghunath, and S. P. S., Eds. Elsevier, 2023, pp. 51–117. [Online]. Available: https://doi.org/10.1016/B978-0-323-90748-4.00012-1

[15] E. Ezugwu, S. Arthur, and E. Hines, "Tool-wear prediction using artificial neural networks," *Journal of Materials Processing Technology*, vol. 49,

no. 3, pp. 255–264, 1995. [Online]. Available: https://doi.org/10.1016/0924-0136(94)01351-Z

[16] C. F. Pérez-Salinas, A. del Olmo, and L. N. López de Lacalle, "Estimation of drag finishing abrasive effect for cutting edge preparation in broaching tool," *Materials*, vol. 15, no. 15, p. 5135, Jul 2022. [Online]. Available: http://dx.doi.org/10.3390/ma15155135

[17] G. Radhakrishnan, C. Kesavan, V. Ramesh, and T. Anandan, "Application of artificial neural network (ANN) for predicting the wear behaviour of Al 2219-SiCp composite," in *Mechanical Engineering Design*, ser. Applied Mechanics and Materials, vol. 852. Trans Tech Publications Ltd, 10 2016, pp. 397–401. [Online]. Available: https://doi.org/10.4028/www.scientific.net/AMM.852.397

[18] B. A. Shuvho, M. A. Chowdhury, and U. K. Debnath, "Analysis of artificial neural network for predicting erosive wear of nylon-12 polymer," *ASTM*, vol. 8, no. 1, 2019. [Online]. Available: https://doi.org/10.1520/MPC20180164

[19] E. Van der Giessen, L. Kubin, and S. Forest, "Jp - foreword," in *Journal De Physique. IV:*, 2001. [Online]. Available: https://bit.ly/48YEgMF

[20] FormLabs, *Tough Resin for Rugged Prototyping*. FormLabs Material Properties, 2018. [Online]. Available: https://bit.ly/45Fi73c

[21] ——, *Standard Materials for High-Resolution Rapid Prototyping*. FormLabs Material Properties, 2017. [Online]. Available: https://bit.ly/407ySTl

[22] B. Sen-Crowe, M. Sutherland, M. McKenney, and A. Elkbuli, "A closer look into global hospital beds capacity and resource shortages during the covid-19 pandemic," *Journal of Surgical Research*, vol. 260, pp. 56–63, 2021. [Online]. Available: https://doi.org/10.1016/j.jss.2020.11.062

[23] V. R. Sastri, "4 - material requirements for plastics used in medical devices," in *Plastics in Medical Devices (Third Edition)*, third edition ed., ser. Plastics Design Library, V. R. Sastri, Ed. William Andrew Publishing, 2022, pp. 65–112. [Online]. Available: https://doi.org/10.1016/B978-0-323-85126-8.00008-4

[24] P. Jacobs, "Fundamentals of stereolithography," *3D Systems Inc.*, pp. 196–210, 1992. [Online]. Available: https://bit.ly/491P2BH

[25] J. H. Lee, R. K. Prudâ€™homme, and I. A. Aksay, "Cure depth in photopolymerization: Experiments and theory," *Journal of Materials Research*, vol. 16, no. 12, pp. 3536–3544, Dec 2001. [Online]. Available: https://doi.org/10.1557/JMR.2001.0485

[26] K. Abd El-Aziz, D. Saber, and A. A. Megahed, "Investigation and prediction of abrasive wear rate of heat-treated HCCIs with different Cr/C ratios using artificial neural networks," *International Journal of Metalcasting*, vol. 15, no. 4, pp. 1149–1163, Oct 2021. [Online]. Available: https://doi.org/10.1007/s40962-020-00547-7

[27] A. Sagbas, F. Kahraman, and U. Esme, "Modeling and predicting abrasive wear behaviour of poly oxy methylenes using response surface methodolgy and neural networks," *Metalurgija*, vol. 48, no. 2, pp. 117–120, 2009. [Online]. Available: https://bit.ly/46WkGif

[28] N. Srivastava, G. Hinton, A. Krizhevsky, I. Sutskever, and R. Salakhutdinov, "Dropout: A simple way to prevent neural networks from overfitting," *Journal of Machine Learning Research*, vol. 15, no. 56, pp. 1929–1958, 2014. [Online]. Available: https://bit.ly/45y1l5W

[29] K. Cho, B. van Merriënboer, D. Bahdanau, and Y. Bengio, "On the properties of neural machine translation: Encoder–decoder approaches," in *Proceedings of SSST-8, Eighth Workshop on Syntax, Semantics and Structure in Statistical Translation*. Doha, Qatar: Association for Computational Linguistics, Oct. 2014, pp. 103–111. [Online]. Available: http://dx.doi.org/10.3115/v1/W14-4012

[30] C. Zhang, S. Bengio, M. Hardt, B. Recht, and O. Vinyals, "Understanding deep learning (still) requires rethinking generalization," *Commun. ACM*, vol. 64, no. 3, pp. 107–115, feb 2021. [Online]. Available: https://doi.org/10.1145/3446776

[31] Y. Zeng, K. Jiang, and J. Chen, "Automatic seismic salt interpretation with deep convolutional neural networks," in *Proceedings of the 2019 3rd International Conference on Information System and Data Mining*. ACM, apr 2019. [Online]. Available: https://doi.org/10.1145%2F3325917.3325926

[32] M. Hawryluk and B. Mrzyglod, "A system of analysis and prediction of the loss of forging tool material applying artificial neural networks," *Journal of Mining and Metallurgy*, vol. 54, no. 3, pp. 323–337, 2018. [Online]. Available: https://doi.org/10.2298/JMMB180417023H

[33] S. Sardar, S. Dey, and D. Das, "Modelling of tribological responses of composites using integrated ANN-GA technique," *Journal of Composite Materials*, vol. 55, no. 7, pp. 873–896, 2021. [Online]. Available: https://doi.org/10.1177/0021998320960520